

MODELING THE WARM IONIZED INTERSTELLAR MEDIUM AND ITS IMPACT ON ELEMENTAL ABUNDANCE STUDIES

KENNETH R. SEMBACH AND J. CHRISTOPHER HOWK

Department of Physics and Astronomy, Johns Hopkins University, 3400 North Charles Street, Baltimore, MD 21218; sembach@pha.jhu.edu, howk@pha.jhu.edu

AND

ROBERT S. I. RYANS AND FRANCIS P. KEENAN

Department of Pure and Applied Physics, Queen's University of Belfast, Belfast, BT7 1NN, Northern Ireland; R.Ryans@qub.ac.uk, F.Keenan@qub.ac.uk

Received 1999 June 14; accepted 1999 August 16

ABSTRACT

We present model calculations of ionization fractions for elements in the warm ($T \sim 10^4$ K), low-density photoionized interstellar medium (WIM) of the Milky Way. We model the WIM as a combination of overlapping low-excitation H II regions having $n(\text{H}^+)/n(\text{H}) \gtrsim 0.8$. Our adopted standard model incorporates an intrinsic elemental abundance pattern similar to that found for warm neutral clouds in the Galaxy and includes the effects of interstellar dust grains. The radiation field is characterized by an ionizing spectrum of a star with $T_{\text{eff}} \approx 35,000$ K and an ionization parameter $\log(q) \approx -4.0$. The emergent emission-line strengths are in agreement with the observed ratios of $[\text{S II}]/\text{H}\alpha$, $[\text{N II}]/\text{H}\alpha$, $[\text{S II}]/[\text{N II}]$, $[\text{O I}]/\text{H}\alpha$, $[\text{O III}]/\text{H}\alpha$, and $\text{He I}/\text{H}\alpha$ in the Galactic WIM. Although the forbidden emission-line intensities depend strongly on the input model parameters, the ionization fractions of the 20 elements studied in this work are robust over a wide range of physical conditions considered in the models. These ionization fractions have direct relevance to absorption-line determinations of the elemental abundances in the warm neutral and ionized gases in the Milky Way and other late-type galaxies. We demonstrate a method for estimating the WIM contributions to the observed column densities of singly and doubly ionized atoms used to derive abundances in the warm neutral gas. We apply this approach to study the gas-phase abundances of the warm interstellar clouds toward the halo star HD 93521.

Subject headings: ISM: abundances — ISM: atoms — H II regions — radiative transfer

1. INTRODUCTION

In elemental abundance studies of the warm, neutral interstellar medium (WNM), it is generally assumed that ionization corrections for photoionized gas are negligible, or at least modest. In practice, this assumption usually takes the form $N(X)/N(\text{H}) \approx N(X^i)/N(\text{H}^0)$, where X^i is the dominant ionization stage of element “ X ” in the neutral gas, even though X^i may also be found in ionized regions (see Savage & Sembach 1996). Ignoring ionized gas contributions to $N(X^i)$ is often justified when studying cold atomic and molecular clouds, but this simplification introduces additional uncertainties into studies of the interstellar medium (ISM) in the immediate vicinity of early-type stars or along extended, low-density sight lines. In these latter cases, ionized material can represent a significant fraction of the total amount of interstellar gas observed and can contribute to the column densities of singly and doubly ionized atoms.

The warm ($T \sim 10^4$ K), ionized interstellar medium (WIM) outside classical H II regions is a fundamental gas-phase constituent of the Milky Way and other late-type spiral galaxies. In the Milky Way, the WIM is detected through faint optical emission-line radiation and pulsar dispersion measures, which together reveal that the ionized gas has an exponential scale height of ~ 1 kpc, a volume-filling factor of $\gtrsim 20\%$, and an average electron density of $\sim 0.1 \text{ cm}^{-3}$ (Reynolds 1993). Though not as easily observed as the H I layer revealed through 21 cm emission, the WIM has a mean mass surface density ($\sim 1.6 M_{\odot} \text{ pc}^{-2}$) nearly one-third that of the H I distribution (Reynolds 1993; Dickey & Lockman 1990). Pervasive warm ionized gas distributions

have been observed in other spiral galaxies besides the Milky Way to varying extents (Dettmar 1990; Rand, Kulkarni, & Hester 1990, 1992; Rand 1996; Hoopes, Walterbos, & Rand 1999). In all cases it seems clear that, while there may be a variety of ionization sources and mechanisms contributing to the WIM emission, photoionization by OB stars is the only source of energy sufficient to maintain the bulk ionization properties of the WIM (which in the Milky Way require $\gtrsim 10^{-4} \text{ ergs cm}^{-2} \text{ s}^{-1}$, or $\sim 15\%$ of the ionizing radiation output from OB stars).

There are two recent observational motivations for modeling the WIM and its impact on elemental abundance studies of the ISM. First, there is an increasing database of emission-line measurements of the WIM. In particular, the Wisconsin H α Mapper (WHAM; Reynolds et al. 1998b) is providing wide sky coverage of H α and other optical emission lines in the diffuse gas. Second, the *Far-Ultraviolet Spectroscopic Explorer* (*FUSE*) will soon produce high spectral resolution absorption-line measurements in the 905–1195 Å bandpass, which contains many diagnostics of photoionized gases. Together with absorption-line data from the *Hubble Space Telescope* Imaging Spectrograph (*HST/STIS*), *FUSE* will enable comprehensive studies of the elemental abundances in the WNM and WIM.

In this paper, we estimate ionization fractions for the WIM based on existing knowledge of its properties. These ionization fractions can be used to derive appropriate corrections for ionized gas contributions to the measured amounts of singly and doubly ionized species found in both the WNM and the WIM. We begin in § 2 by summarizing the current observational constraints on the WIM. In § 3 we

describe our model of the WIM, its boundary conditions, the parameter space explored, and the sensitivity of the predicted emission-line ratios and ionization fractions to the input parameters. In § 4 we provide a short description of the applicability of the model results to absorption-line studies of elemental abundances in the ISM. § 5 contains a brief discussion of these results and a few concluding remarks. Ionization fractions for radially averaged sight lines through low-density H II regions can be found in the Appendix.

2. EMISSION-LINE PROPERTIES OF THE WARM IONIZED MEDIUM

The primary optical emission lines used to characterize the WIM are H α λ 6563, [S II] λ 6716, [N II] λ 6583, [O I] λ 6300, [O III] λ 5007, and He I λ 5876. We compile a set of measurements of these species appearing in the literature in Table 1, where we list the line intensities normalized to the observed H α intensity. Compared to classical H II regions, the WIM has high [N II]/H α and [S II]/H α and low [O III]/H α ratios (Reynolds 1985b; Osterbrock 1989). A subset of the listed ratios has been modeled and discussed by Domgörgen & Mathis (1994), who found that dilute stellar radiation leaking through the ISM provides an adequate source of ionization for the WIM. This paradigm is supported by models of the radiative transfer of ionizing photons through the Galaxy subject to the presence of interstellar clouds (Miller & Cox 1993; Dove & Shull 1994; Bland-Hawthorn & Maloney 1999). Additional secondary ionizing sources may be present; in at least one case (Ogden & Reynolds 1985), the emission from a filament within the diffuse background emission appears to be due to collisional ionization by a weak shock. However, the large [N II]/H α ratio is atypical of the more general value of 0.4–0.6 for the emission observed in other directions (see Table 1).

The emission-line ratios for gas in the Local and Perseus spiral arms change significantly as a function of the observed H α intensity (Haffner, Reynolds, & Tufte 1999). Ratios of [S II]/H α and [N II]/H α in excess of unity are seen in some directions where $I_{\text{H}\alpha} < 0.5R$. The ranges of [S II]/H α and [N II]/H α listed in Table 1 for the Perseus

arm encompass a majority of the observed values and are appropriate for heights $z \lesssim 1.0$ kpc above the Perseus arm. Haffner et al. (1999) argue that the [N II]/H α ratio probes the temperature of the gas while the [S II]/[N II] ratio traces the ionization state of sulfur. (The [S II]/H α ratio is therefore a probe of both physical properties.) They interpret the large, systematic increase in [N II]/H α with height above the plane as an indicator of increasing temperature, with an as yet unidentified source of heating at large distances from the Galactic midplane. Extragalactic background radiation is an unlikely source, since the ionizing flux out to about 100 kpc from the Galactic disk is dominated by light from the Galaxy (Maloney & Bland-Hawthorn 1999). Interestingly, even though the [S II]/H α and [N II]/H α ratios change by more than a factor of 3 with height above the plane in the Perseus arm, the ratio [S II]/[N II] ≈ 0.5 –0.65 is relatively constant and shows virtually no dependence on height above the Galactic midplane. Thus, in the interpretation presented by Haffner et al., the increase in temperature with height above the plane is not matched by corresponding changes in the ionization state of the gas.

To date, the strongest constraints on the ionization of the WIM come from [O I] λ 6300, [O III] λ 5007, and He I λ 5876 emission-line observations (see Domgörgen & Mathis 1994). A complete set of optical emission-line measurements is not yet available even for a single direction; we make the simplifying assumption that the range in values and upper limits listed in Table 1 is representative of the WIM as a whole. However, we also recognize that a range of physical conditions is possible and allow the model parameters to vary accordingly. It is hoped that additional emission-line data in the near future will lead to a better description of the intensities of the less well studied species.

3. MODEL DESCRIPTION

To study the physical conditions of the Galactic WIM, we use the ionization equilibrium code CLOUDY (Version 90.04; described by Ferland et al. 1998; Ferland 1996) to derive the temperature and ionization structure of spherically symmetric nebulae surrounding single ionizing sources. We model the WIM as a combination of low-density, low-excitation H II regions. Our goal is to estimate

TABLE 1
EMISSION-LINE MEASUREMENTS OF THE WARM IONIZED MEDIUM

Direction (l, b)	$\frac{[\text{S II}]}{\text{H}\alpha}$	$\frac{[\text{N II}]}{\text{H}\alpha}$	$\frac{[\text{O I}]}{\text{H}\alpha}$	$\frac{[\text{O III}]}{\text{H}\alpha}$	$\frac{\text{He I}}{\text{H}\alpha}$	Reference
96°0, 0°0	0.29 \pm 0.05	0.28 \pm 0.06	...	0.058 \pm 0.025	...	1, 2
114°0, 0°0	0.24 \pm 0.04	...	0.020 \pm 0.003	...	<0.02	2, 3, 4
130°0, 0°0	0.27 \pm 0.06	...	0.028 \pm 0.009	2, 3
184°4, -0°6 and 186°0, 0°0	0.23 \pm 0.04	0.21 \pm 0.02	...	<0.06	...	2, 5
194°0, 0°0	0.38 \pm 0.05	0.44 \pm 0.05	...	0.068 \pm 0.025	<0.02	1, 2, 4
97°3, -29°7 and 97°7, -26°7	0.39 \pm 0.11	<0.20	...	1, 2
144°0, -21°0 (weak shock)	0.44	0.70	< 0.12	<0.57	...	6
123°–164°, -6° to -35° (Perseus Arm).....	0.2–0.4 ^a	0.4–0.6 ^a	<0.012 ^b	3, 7
			0.044 \pm 0.011 ^b			

^a The ranges of values quoted are appropriate for Perseus arm gas within $\lesssim 1$ kpc of the Galactic plane having an H α intensity of ~ 2 –3R. There is a slightly larger scatter to higher values in the Local arm gas in the same directions. Both the [S II]/H α and [N II]/H α ratios are anticorrelated with $I_{\text{H}\alpha}$. The upper envelope of observed ratios extends to values several times higher than those listed.

^b These values are for two velocities (-60 and -31 km s⁻¹) at the position $l = 130^\circ, b = -7^\circ 5'$.

REFERENCES.— (1) Reynolds 1985b; (2) Reynolds 1985a; (3) Reynolds et al. 1998a; (4) Reynolds & Tufte 1995; (5) Reynolds, Roessler, & Scherb 1977; (6) Ogden & Reynolds (1985), (7) Haffner et al. 1999.

the ionization fractions, $x(X^i) \equiv N(X^i)/N(X)$, of several ionization stages, i , of the most important elements, X , for studying the gas-phase abundances of the Galactic ISM. In doing so we endeavor to match the observed emission-line observations of the WIM as closely as possible.

3.1. Approach and Assumptions

Following Domgörgen & Mathis (1994), we model the WIM of the Galaxy as a combination of low-density H II regions. Our models calculate the temperature and ionization structure of the model H II region from a distance of 0.3 pc from the exciting source to the point where the fraction of neutral hydrogen, $x(\text{H}^0)$, at the edge of the nebula becomes larger than a critical value x_{edge} . Domgörgen & Mathis (1994) used models with $x_{\text{edge}} = 0.10$ to approximate fully ionized material and models with $x_{\text{edge}} = 0.95$ to simulate ionized interfaces of neutral clouds or other regions with a significant fraction of neutral hydrogen. For continuity with their work, we consider the same x_{edge} values in this study. In some situations, x_{edge} values as high as 1.00 may be encountered as the sight line passes into a fully neutral cloud, but the model results for $x_{\text{edge}} = 0.95$ closely approximate those for $x_{\text{edge}} = 1.00$. The emission-line intensities of the gas in these two cases are indistinguishable, and the ionization fractions vary by less than $\sim 10\%$ for most ions. In this study we also consider a hybrid gas mixture described by a linear combination of equal amounts of $x_{\text{edge}} = 0.10$ gas and $x_{\text{edge}} = 0.95$ gas.

The characteristics of a low-density photoionized nebula are uniquely determined by three input parameters, assuming a given set of atomic data. These parameters are the set of gas-phase abundances adopted for elements heavier than hydrogen, the shape of the ionizing spectrum, and the ionization parameter q , which is a measure of the ratio of ionizing photons to particles in the nebula (see Domgörgen & Mathis 1994; Howk & Savage 1999). The inclusion of dust grain heating and cooling can also affect the model results, but these effects are small in the models considered (see § 3.3).

We consider three sets of abundances in our models: solar system, B star, and warm neutral interstellar medium values, all of which are summarized in Table 2. The abundance of He is assumed to be 1/10 the abundance of H in all three cases. The solar system abundances are meteoritic values from Anders & Grevesse (1989), except for C, N, and O, which are photospheric values from Grevesse & Noels (1993). The B star abundances, which may represent a better “cosmic” reference system than solar system abundances (see, e.g., Savage & Sembach 1996; Mathis 1996), are averages of the Kilian-Montenbruck, Gehren, & Nissen (1994) determinations. We assume that the B star abundances of elements lacking observed values are equal to the solar values scaled downward by 0.2 dex. We also consider a WNM-like abundance pattern to account for the possible effects of elemental incorporation into dust grains in the ionized interstellar medium. The elemental depletion pattern inferred for the WIM is comparable to that observed in the WNM (Howk & Savage 1999; see also Lagache et al. 1999). We adopt WNM gas-phase abundances equal to those observed in the well-studied warm diffuse clouds toward the low-halo star μ Columbae (Howk, Savage, & Fabian 1999). The observed abundances in these clouds exhibit the imprint of elemental incorporation into dust grains. We adopt C, N, and O abundances for the

TABLE 2
IONIZATION POTENTIALS AND REFERENCE ABUNDANCES

ELEMENT	IONIZATION POTENTIALS (eV) ^a			$A(X)$ ^b		
	I	II	III	Solar	B Star	WNM
H.....	13.60	12.00	12.00	12.00
He.....	24.59	54.42	...	11.00	11.00	11.00
C.....	11.26	<u>24.38</u>	<u>47.89</u>	8.55	8.27	8.15
N.....	<u>14.53</u>	<u>29.60</u>	<u>47.45</u>	7.97	7.80	7.88
O.....	<u>13.62</u>	35.12	54.93	8.87	8.56	8.50
Ne.....	21.56	40.96	63.45	8.07	8.20	8.07
Na.....	5.14	47.29	71.64	6.31	6.11 [†]	6.11
Mg.....	<u>7.65</u>	<u>15.04</u>	80.14	7.58	7.38	7.16
Al.....	5.99	<u>18.83</u>	<u>28.45</u>	6.48	6.19	5.18
Si.....	8.15	<u>16.34</u>	<u>33.49</u>	7.55	7.20	7.18
P.....	10.49	<u>19.72</u>	<u>30.18</u>	5.57	5.37 [†]	5.37
S.....	10.36	<u>23.33</u>	<u>34.83</u>	7.27	6.97	7.07
Ar.....	<u>15.76</u>	<u>27.63</u>	40.74	6.52	6.32 [†]	6.32
Ca.....	6.11	11.87	50.91	6.36	6.16 [†]	5.06
Ti.....	6.82	13.58	27.49	4.93	4.73 [†]	3.86
Cr.....	6.77	<u>16.50</u>	<u>30.96</u>	5.68	5.48 [†]	4.55
Mn.....	7.43	<u>15.64</u>	33.67	5.53	5.33 [†]	4.56
Fe.....	7.87	<u>16.18</u>	<u>30.65</u>	7.51	7.40	6.21
Ni.....	7.64	<u>18.17</u>	35.17	6.25	6.05 [†]	4.95
Zn.....	9.39	<u>17.96</u>	39.72	4.65	4.45 [†]	4.45

^a Ionization potentials are from Moore 1970. Underlined values indicate that the ionization stage has at least one ground-state resonance line in the *FUSE/HST* ultraviolet bandpass (912–3000 Å) that could be observable in the WIM.

^b Reference abundances are logarithmic values on a scale where $A(X) = \log(X/H) + 12.00$. Solar abundances are meteoritic values from Anders & Grevesse 1989, except for C, N, and O, which are photospheric values from Grevesse & Noels 1993. B star abundances are from Kilian-Montenbruck et al. 1994, except for those cases marked with a dagger, which are equal to the solar value minus 0.2 dex. The WNM abundances are equal to the solar abundances modified by dust as observed in the warm diffuse clouds toward μ Columbae by Howk et al. 1999. WNM values for C, N, and O are from Sofia et al. 1997, Meyer et al. 1997, and Meyer et al. 1998, respectively.

WNM from Sofia et al. (1997), Meyer, Cardelli, & Sofia (1997), and Meyer, Jura, & Cardelli (1998), respectively.

Our models are unable to match the $[\text{S II}]/[\text{N II}]$ ratios observed by Haffner et al. (1999) if we adopt a solar abundance for sulfur. The predicted values of $[\text{S II}]/[\text{N II}]$ are too high by roughly a factor of 1.5. We have explored possible explanations for high $[\text{S II}]/[\text{N II}]$ ratios within the context of our model but find that the most reasonable explanation is a subsolar sulfur reference abundance. (Haffner et al. 1999 reached a similar conclusion.) The μ Columbae clouds exhibit nearly solar gas-phase abundances of the nondepleted elements S, Zn, and P, but this sight line may be unusual in this respect (Howk et al. 1999). Therefore, for the elements S, Zn, P, Ar, and Na we adopt WNM reference abundances equal to the solar system values scaled downward by 0.2 dex, in agreement with our current understanding of the abundances in the local ISM (Mathis 1996; Snow & Witt 1996; Meyer et al. 1998). This is essentially equivalent to adopting a B star reference abundance with minimal incorporation of these elements into interstellar dust grains.

All the H II region models calculated with the adopted WNM abundances include a standard mixture of interstellar graphite and silicate grains (see Ferland 1996; Baldwin et al. 1991). Dust grains in the model nebulae affect the thermal structure of the medium through photoelectric

heating. The grain opacity also alters the shape of the ionizing spectrum slightly. The incorporation of potential coolants into grains is an essential component of the model and is required to match the observed emission-line strengths.

We use ATLAS line-blanketed LTE stellar atmosphere models (Kurucz 1991) as input spectra to the CLOUDY ionization code. The input spectral shape is varied by changing the effective temperature of the stellar atmosphere of the central ionizing source. We consider model H II regions ionized by central stars with stellar effective temperatures in the range $31,000 \leq T_{\text{eff}} \leq 41,000$ K.

The third input to our models, the ionization parameter, is a dimensionless measure of the relative particle and ionizing photon densities. Throughout this work we write the ionization parameter q in the form

$$q \equiv n_{\text{H}} f^2 L_{50}, \quad (1)$$

where L_{50} is the stellar ionizing luminosity in units of 10^{50} photons s^{-1} and f is the volume-filling factor of the ionized gas (Domgörgen & Mathis 1994). This definition of the ionization parameter q is related to the “volume-averaged” ionization parameter, $U = \frac{1}{3} \langle n_{\gamma}/n_e \rangle$, through

$$q = (10^{-50}) \left(\frac{36\pi c^3}{\alpha_B^2} \right) U^3 \\ = (1.33 \times 10^{-50}) \left(\frac{\pi c^3}{\alpha_B^2} \right) \left\langle \frac{n_{\gamma}}{n_e} \right\rangle^3, \quad (2)$$

where α_B is the recombination coefficient of H to levels $n \geq 2$ and n_{γ} is the number density of ionizing photons.

Bright high-density H II regions typically have values of $\log(q) \gtrsim -1.0$. We calculate models over the range $-4.0 \lesssim \log(q) \lesssim -3.0$, which is more appropriate for the low-density WIM (Domgörgen & Mathis 1994). For a nebula surrounding a normal O9 V star with $T_{\text{eff}} = 35,000$ K, total luminosity $\log L_*/L_{\odot} = 5.0$, and ionizing photon flux $\log L_{50} \approx -1.6$ (Vacca, Garmany, & Shull 1996), a value $\log(q) = -4.0$ corresponds to $n_e f^2 \approx 4 \times 10^{-3} \text{ cm}^{-3}$. Estimates for the density of the WIM typically yield $n_e \sim 0.08$ and $f \gtrsim 0.20$ (Reynolds 1993). Note that the ionization parameter rather than the density determines the properties of the model nebulae; for a given value of q in equation (2), higher values of n_e can be achieved provided there is a proportional change in n_{γ} .

We extract from our models the volume-averaged intensities of various emission lines relative to H α as well as the ionization fractions, $x(X^i)$, of elements important for

absorption-line studies of the low-density Galactic ISM.¹ We use volume-weighted averages rather than radial averages since a random, extended sight line through the WIM is likely to sample gas found within a variety of low-density ionized regions. The predicted emission-line ratios can be compared directly with observations of the Galactic WIM (§ 2), while the ionization fractions are useful for analyzing absorption-line data.

Several caveats regarding these models are worth mentioning. First, the atomic data incorporated in CLOUDY, while extensive, is incomplete. For example, the low-temperature dielectronic recombination coefficients for most elements in the third and fourth rows of the periodic table are estimated (Ferland 1996; Ferland et al. 1998). For some elements this recombination pathway can be a significant contributor to the ionization balance at nebular temperatures. Although the atomic data are somewhat incomplete for many of the elements considered, we believe it is important to include the current best values of the ionization fractions of all the elements that might be of interest. Second, some of the emission-line predictions used to match the WIM observations are highly sensitive to the predicted temperature of the medium (Osterbrock 1989). We discuss this further in § 3.3. CLOUDY calculates the thermal equilibrium structure of model nebulae, but there may be additional heating and cooling processes in the WIM that are not taken into account in the models. We assume that the WIM is photoionized purely by stellar continuum radiation (as well as by diffuse radiation from the nebular gas itself). Other processes may play a secondary role in ionizing the WIM, such as magnetic reconnection, dissipation of turbulence, or the mixing of cool material with hot, collisionally ionized gas (Raymond 1992; Slavin, Shull, & Begelman 1993; Minter & Balser 1997).

3.2. The Standard Model

The parameter space explored by our models spans a wide range of physical properties in the ionized gas. Our preferred model for the WIM, hereafter referred to as the “standard model,” assumes WNM-like abundances with interstellar grains included. The ionizing spectrum is that of a 35,000 K star, consistent with the upper limits to the He I 5876 Å line emission set by observations (Reynolds & Tufté 1995). We assume a very dilute radiation field characterized by $\log(q) = -4.0$.

¹ All emission-line ratios in this paper are intensity ratios, where the intensities are measured in energy units, not photon units.

TABLE 3
STANDARD MODEL WIM EMISSION LINES

LINE	VOLUME-AVERAGED INTENSITY RATIO $\left(\frac{I_{\lambda}}{I_{\text{H}\alpha}} \right)$			OBSERVED ^a
	$x_{\text{edge}} = 0.10$	$x_{\text{edge}} = 0.95$	Composite ^b	
[S II] $\lambda 6716$	0.258	0.325	0.292	0.2–0.4
[N II] $\lambda 6583$	0.439	0.462	0.451	0.3–0.6
[O I] $\lambda 6300$	0.005	0.021	0.013	0.01–0.03
[O III] $\lambda 5007$	0.002	0.002	0.002	$\lesssim 0.1$
He I $\lambda 5876$	0.017	0.013	0.015	< 0.02

^a This summary of observed intensity ratios is based on the data listed in Table 1.

^b The composite model is comprised of equal amounts of $x_{\text{edge}} = 0.10$ and $x_{\text{edge}} = 0.95$ material.

Table 3 contains the emission-line intensities relative to $H\alpha$ predicted by our CLOUDY models. We give values for the $x_{\text{edge}} = 0.10$, $x_{\text{edge}} = 0.95$, and standard composite models. The composite model provides a reasonable description of the observed emission-line ratios, with the possible exceptions of $[\text{O I}] \lambda 6300/H\alpha$ and $[\text{O III}] \lambda 5007/H\alpha$. The standard model produces less $[\text{O III}]$ emission relative to $H\alpha$ than is suggested by the observations. This is a common feature of our models. The predicted $[\text{O I}]/H\alpha$ ratio may also be slightly low compared to the observed values (see Table 1). While most directions have observable

values of $[\text{O I}]/H\alpha \sim 0.02$, our composite models typically predict $\lesssim 0.015$. The strength of the $[\text{O I}] \lambda 6300 \text{ \AA}$ line, however, is strongly dependent on the temperature of the medium (Reynolds et al. 1998a).

We are not overly concerned about the possible underproduction of $[\text{O III}] \lambda 5007$ relative to $H\alpha$ in our models compared with the observed upper limit of $\lesssim 0.1$. This observational limit was derived by noting that the current observed values (Table 1) are at best 2–3 σ detections, so the actual value may be considerably lower than this limit. Enhanced $[\text{O III}]$ emission can be produced by alternate mechanisms (e.g., shocks) as well as by photoionization, so we expect that the observed values should indeed provide a conservative upper bound for the model predictions.

Previous investigations seeking to model the WIM emission-line properties (e.g., Domgörgen & Mathis 1994) predicted higher $[\text{O I}] \lambda 6300$ and $[\text{O III}] \lambda 5007$ emission than our standard model. To disentangle the differences between these earlier works and our models, we have calculated CLOUDY models with the abundances, ionizing spectrum, and ionization parameter adopted by Domgörgen & Mathis. We compare their predicted emission-line ratios with those from our CLOUDY models in Table 4 and find good agreement in most cases. The slight remaining discrepancies, particularly those for $[\text{O III}]$, are probably due to differences in the atomic data used in the models (Ferland et al. 1998). The elements included in the models compared in Table 4 were limited to H, He, N, O, Ne, and S. As a result, the cooling is less efficient than in our standard model, which incorporates elements up through Zn, and the resulting nebular temperatures are higher in the Domgörgen & Mathis models ($T_{\text{neb}} \sim 8000 \text{ K}$ vs. $T_{\text{neb}} \sim 6700 \text{ K}$ in our standard model). An extensive

TABLE 4
EMISSION-LINE COMPARISON

LINE	INTENSITY RATIO ^a $\left(\frac{I_\lambda}{I_{H\alpha}}\right)$	
	CLOUDY ($T_{\text{neb}} = 8040 \text{ K}$) ^b	DM94 ($T_{\text{neb}} = 8200 \text{ K}$) ^b
[S II] $\lambda 6716$	0.77	0.66
[N II] $\lambda 6583$	0.37	0.37
[O I] $\lambda 6300$	0.051	0.055
[O II] $\lambda 3727$	1.17	1.18
[O III] $\lambda 5007$	0.009	0.038
He I $\lambda 5876$	0.025	0.029

^a These volume-averaged intensity ratios are predictions from the CLOUDY and Domgörgen & Mathis (1994) ionization codes for a model nebula with $x_{\text{edge}} = 0.95$, $T_{\text{eff}} = 38,000 \text{ K}$, and $\log(q) = -4.0$. The calculations included H, He, N, O, Ne, and S scaled to the Orion abundances from Peimbert, Torres-Peimbert, & Ruiz (1992).

^b Volume-averaged nebular temperature defined by $T_{\text{neb}} = \int T n_e dV / \int n_e dV$.

TABLE 5
IONIZATION FRACTIONS FOR THE STANDARD MODEL^{a,b}

ELEMENT	$x_{\text{edge}} = 0.10$			$x_{\text{edge}} = 0.95$			COMPOSITE ^c		
	I	II	III	I	II	III	I	II	III
H	-1.30	-0.02	...	-0.49	-0.17	...	-0.73	-0.09	...
He	-0.17	-0.50	...	-0.07	-0.83	...	-0.12	-0.63	...
C	-2.24	-0.02	-1.31	-2.16	-0.01	-1.63	-2.20	-0.02	-1.44
N	-1.33	-0.03	-1.72	-0.52	-0.16	-2.05	-0.76	-0.09	-1.85
O	-1.26	-0.03	-2.74	-0.48	-0.18	-3.07	-0.71	-0.09	-2.87
Ne	-0.97	-0.05	-3.88	-0.54	-0.15	-4.21	-0.70	-0.10	-4.02
Na	-1.93	-0.01	-5.53	-1.75	-0.01	-5.82	-1.83	-0.01	-5.65
Mg	-2.30	-0.15	-0.54	-2.22	-0.07	-0.82	-2.26	-0.11	-0.66
Al	-2.81	-0.03	-1.16	-2.83	-0.02	-1.44	-2.82	-0.03	-1.28
Si	-3.63	-0.06	-0.92	-3.51	-0.03	-1.23	-3.57	-0.04	-1.05
P	-2.39	-0.09	-0.72	-2.36	-0.05	-1.01	-2.37	-0.07	-0.84
S	-2.83	-0.11	-0.65	-2.76	-0.06	-0.90	-2.80	-0.09	-0.75
Ar	-1.86	-0.12	-0.63	-0.94	-0.11	-0.96	-1.19	-0.12	-0.77
Ca	-2.33	-0.71	-0.10	-2.31	-0.65	-0.11	-2.32	-0.68	-0.10
Ti	-3.19	-0.34	-0.28	-2.87	-0.15	-0.54	-3.00	-0.23	-0.39
Cr	-3.42	-0.41	-0.21	-3.12	-0.17	-0.48	-3.24	-0.28	-0.33
Mn	-1.68	-0.31	-0.31	-1.39	-0.16	-0.58	-1.51	-0.23	-0.43
Fe	-3.41	-0.47	-0.19	-3.02	-0.19	-0.45	-3.17	-0.31	-0.30
Ni	-1.98	-0.11	-0.68	-1.89	-0.05	-1.00	-1.93	-0.08	-0.81
Zn	-2.15	-0.04	-1.08	-1.96	-0.02	-1.40	-2.05	-0.03	-1.21

^a The ionization fraction of an ion X^i is given by $x(X^i) = N(X^i)/N(X_{\text{total}})$. We present volume-averaged values of $\log x(X^i)$ for the first three ionization states of each element.

^b The standard model assumes WNM abundances (see Table 1), $\log(q) = -4.0$, and a stellar input spectrum characterized by $T_{\text{eff}} = 35,000 \text{ K}$ and $\log(g) = 4.0$.

^c The composite model is comprised of equal amounts of $x_{\text{edge}} = 0.10$ and $x_{\text{edge}} = 0.95$ material.

comparison of CLOUDY to other ionization codes can be found in Ferland et al. (1994).

We present volume-averaged ionization fractions for the standard model in Table 5. Values of $x(X^i)$ are listed for the first three ionization stages of 20 elements. Ionization potentials can be found in Table 2, where we have underlined those ionization stages that have at least one observable resonance line in the 912–3000 Å bandpass suitable for high-resolution ultraviolet absorption-line work. In the standard composite model, hydrogen is almost fully ionized, $x(\text{H}^+) = 0.81$.

3.3. Sensitivity of Emission-Line Ratios to Model Parameters

The emission-line ratios predicted by our models have varying sensitivities to the input model parameters (abundance, ionizing spectrum, and ionization parameter). In Figure 1 we illustrate the dependences of the emission-line ratios on the effective temperature of the central ionizing source and the abundance pattern adopted for models

with $\log(q) = -4.0$. The shaded regions indicate the ranges of observed values as summarized in Table 3. We have included $[\text{O II}] \lambda 3727$ for completeness, though this line has not yet been observed in the Galactic WIM. Of the lines studied, $[\text{S II}] \lambda 6716$ and $[\text{O I}] \lambda 6300$ are the most sensitive to the adopted set of abundances. $\text{He I } \lambda 5876$ and $[\text{O III}] \lambda 5007$ are affected only slightly by the chosen abundances but vary by at least an order of magnitude over the effective temperature range plotted. $[\text{S II}] \lambda 6716$ and $[\text{N II}] \lambda 6583$ are the least sensitive to the ionizing spectrum, varying by less than a factor of 2 over the same range.

The upper limit to the $\text{He I}/\text{H}\alpha$ ratio implies that the ionizing spectrum of the WIM produces a ratio of He- to H-ionizing photons less than that produced by an O star with $T_{\text{eff}} \lesssim 36,000$ K (Reynolds & Tufté 1995). The observed $[\text{O I}]/\text{H}\alpha$ constraint is barely satisfied over this range of stellar effective temperatures, which indicates that there may be some additional nebular heating required to increase the predicted $[\text{O I}]$ emission. Note, however, that $[\text{O I}]$ measurements exist for a small number of WIM sight

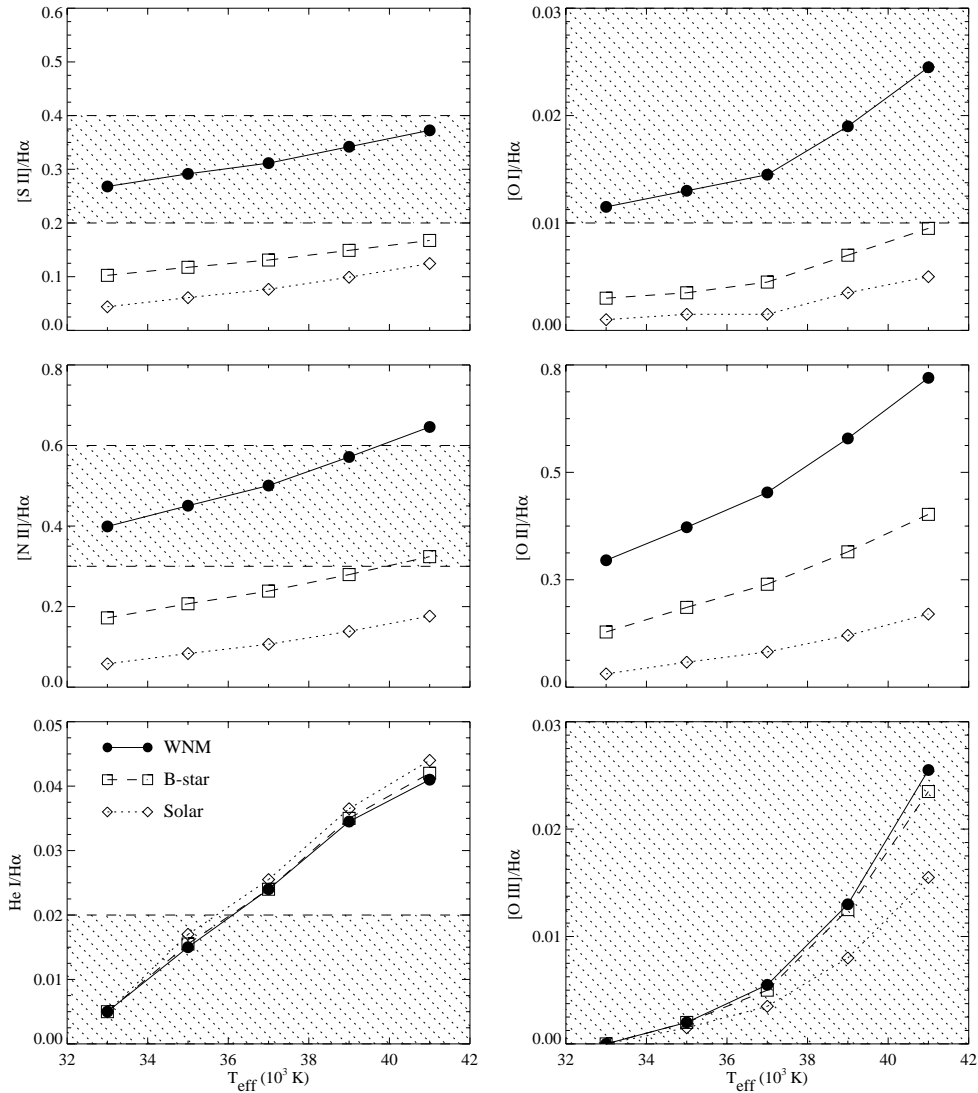


FIG. 1.—Predicted emission-line ratios vs. the assumed effective temperature of the underlying stellar ionizing source from the CLOUDY model nebula calculations. The three curves in each panel depict the relationships for the different abundance patterns (see legend in bottom left panel). For each set of reference abundances we show the composite model with an ionization parameter $\log(q) = -4.0$. Shaded regions indicate the range of observed emission-line ratios (see Table 1). Note that $[\text{O II}] \lambda 3727$ emission has not yet been observed in the WIM.

TABLE 6
EFFECTS OF NEBULAR TEMPERATURE ON EMISSION LINES

LINE	INTENSITY RATIO ^a $\left(\frac{I_\lambda}{I_{H\alpha}}\right)$		
	6000 K	8000 K	10000 K
[S II] $\lambda 6716$	0.200	0.539	0.990
[N II] $\lambda 6583$	0.291	0.820	1.571
[O I] $\lambda 6300$	0.009	0.032	0.075
[O III] $\lambda 5007$	0.001	0.002	0.005
He I $\lambda 5876$	0.016	0.015	0.014
[O II] $\lambda 3727$	0.186	1.050	3.031
[S III] $\lambda 9532$	0.085	0.173	0.271

^a These volume-averaged intensity ratios are for the standard composite model, which is comprised of equal amounts of $x_{\text{edge}} = 0.10$ and $x_{\text{edge}} = 0.95$ material.

lines, and there appears to be a significant variation in the [O I]/H α ratio between these directions. The assumption that these emission-line ratios are representative of the WIM as a whole needs to be confirmed observationally.

The average nebular electron temperature in our standard model is $T_{\text{neb}} = 6700$ K, which is determined by the input model parameters and the detailed physics of heating and cooling in the nebula. We tabulate the effects of nebular temperature on the emission-line ratios for the standard composite model in Table 6, where we have forced T_{neb} to be uniform throughout our model nebulae at temperatures of 6000, 8000, and 10,000 K. The recombination-line ratio He I/H α is relatively unaffected by nebular temperature, as expected, but the forbidden emission lines vary greatly in strength as a function of T_{neb} . Changes of ~ 500 –1000 K in T_{neb} can increase [O I]/H α by a factor of ~ 2 . In general, values of T_{neb} as high as 8000 K are inconsistent with the observations in Table 3. However, the observed increase in [N II]/H α and [S II]/H α with height above the Galactic plane suggests temperatures as high as $T_{\text{neb}} \sim 10^4$ K may be appropriate at large z distances (Haffner et al. 1999). Observations of [O II] $\lambda 3727$ could provide an excellent test for additional heating sources since the [O II]/H α ratio is expected to vary by a factor of about 16 for 6000 K $\lesssim T_{\text{neb}} \lesssim 10,000$ K.

We note that grain heating in our models is approximately balanced by grain cooling under the conditions considered. The heating rate due to ejection of photoelectrons from grains is less than 10% of the H I bound-free photoionization heating in our models. We refer the reader to Cox & Reynolds (1992) and Baldwin et al. (1991) for additional discussions of grain heating in the ionized ISM.

In general, the emission-line ratios do not depend strongly on the value of q adopted for the standard model. A value of $\log(q) = -3.5$ versus -4.0 results in changes of less than 10% for [N II]/H α , [S II]/H α , [O I]/H α , and He I/H α . The [O III]/H α ratio varies by less than $\sim 40\%$, with smaller changes occurring for values of $T_{\text{eff}} < 38,000$ K.

3.4. Sensitivity of Ionization Fractions to Model Parameters

The ionization fractions for the standard model (Table 5) have modest dependencies on the input parameters used to model the emission-line observations. We illustrate these dependencies in Figures 2 and 3, where we plot the ionization fractions as functions of T_{eff} and $\log(q)$, respectively. The standard $x_{\text{edge}} = 0.10$, $x_{\text{edge}} = 0.95$, and composite models are shown with dashed, dotted, and solid lines,

respectively. The ionization stages are differentiated by the type of symbol used, with open circles for neutral species, filled circles for singly ionized species, and crossed circles for doubly ionized species. For a few ions, the ionization fractions depend strongly on T_{eff} (e.g., He I, He II, and C III), but in most other cases of interest here, the variations with T_{eff} are modest [$\Delta \log x(X^i) \leq 0.2$ dex]. Similarly, changes in the adopted reference abundances do not change the ionization fractions significantly. The variations of $\log x(X^i)$ with $\log(q)$ shown in Figure 3 are typically less than 0.2 dex for values of $\log(q)$ between -4.0 and -3.0 .

The ionization fractions do not depend significantly on the nebular temperature since their values are governed in large part by recombination processes. Changes in $x(X^i)$ are less than $\sim 10\%$ for $T_{\text{neb}} = 6000$ –10,000 K. The lack of variation in the strength of the permitted He I $\lambda 5876$ recombination line relative to H α with nebular temperature is another manifestation of this insensitivity (see Table 6).

The information provided in Table 5 and Figures 2 and 3 should have a broad range of applicability to studies of the WNM and WIM. The ionization fractions can be scaled easily to other preferred values of the input model parameters. As better emission-line data become available and additional constraints are set on the properties of the WIM, the standard model ionization fractions can also be refined using the information presented here.

4. APPLICATION TO ABSORPTION-LINE ABUNDANCE STUDIES OF THE WNM AND WIM

4.1. Methodology

In this section we outline a simple strategy for estimating elemental abundances in the warm neutral and ionized media of the Galaxy. For simplicity, any cold neutral gas along the sight line can be considered as WNM material in the following discussion. Many singly ionized elements can be found in both the WNM and the WIM (e.g., Al II, Si II, P II, S II, Fe II), making it necessary to account for the relative contributions of each type of gas to the observed column densities. Higher ionization stages are preferentially found in the WIM, and these can be used to isolate the elemental abundances in the WIM.

Assume that an ion X^j is found only in the ionized gas and presumably has no appreciable abundance in the WNM (e.g., S^{+2}). Then, we have

$$\begin{aligned} N(X^i)_{\text{WIM}} &= N(X^i), \quad (i \geq j), \\ N(X^i)_{\text{WNM}} &= 0, \end{aligned} \quad (3)$$

where $N(X^i)$ is the observed column density of X^i . In general, the total amount of an ion is the sum of contributions from the WIM and WNM:

$$N(X^i) = N(X^i)_{\text{WIM}} + N(X^i)_{\text{WNM}}. \quad (4)$$

The column density of element X in the WIM is given by

$$N(X)_{\text{WIM}} = N(X^j)/x(X^j), \quad (5)$$

where $x(X^j)$ is the volume-averaged ionization fraction found in Table 5. The ionization fractions in Table 5 are appropriate for the average properties of the WIM. The corresponding logarithmic abundance of the element relative to hydrogen in the WIM is

$$A(X)_{\text{WIM}} = \log \left| \frac{N(X)}{N(H)} \right|_{\text{WIM}} + 12.00. \quad (6)$$

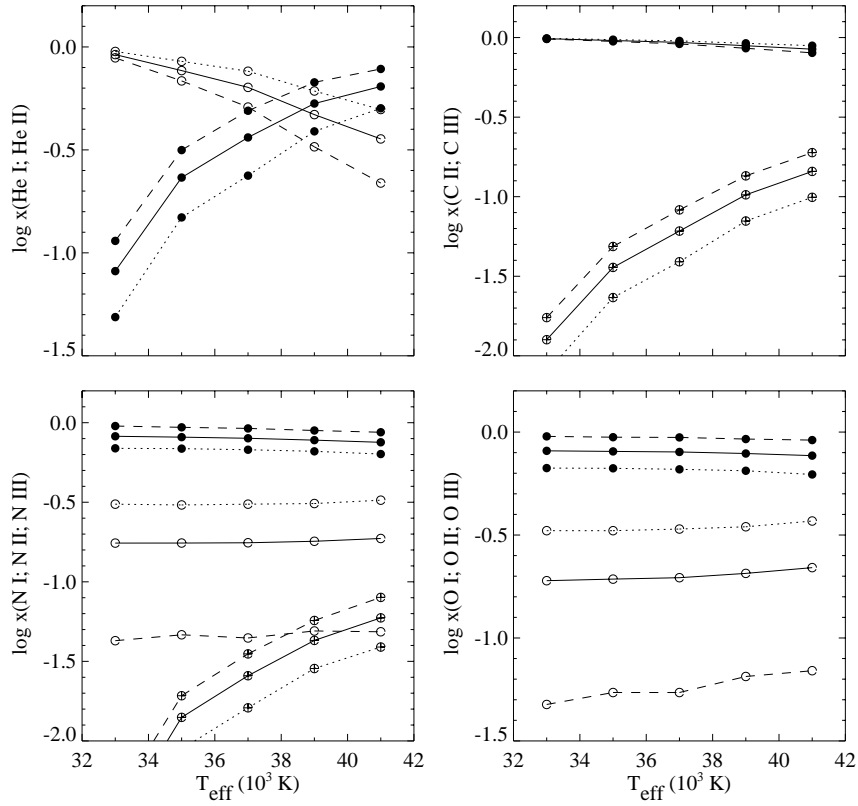


FIG. 2a

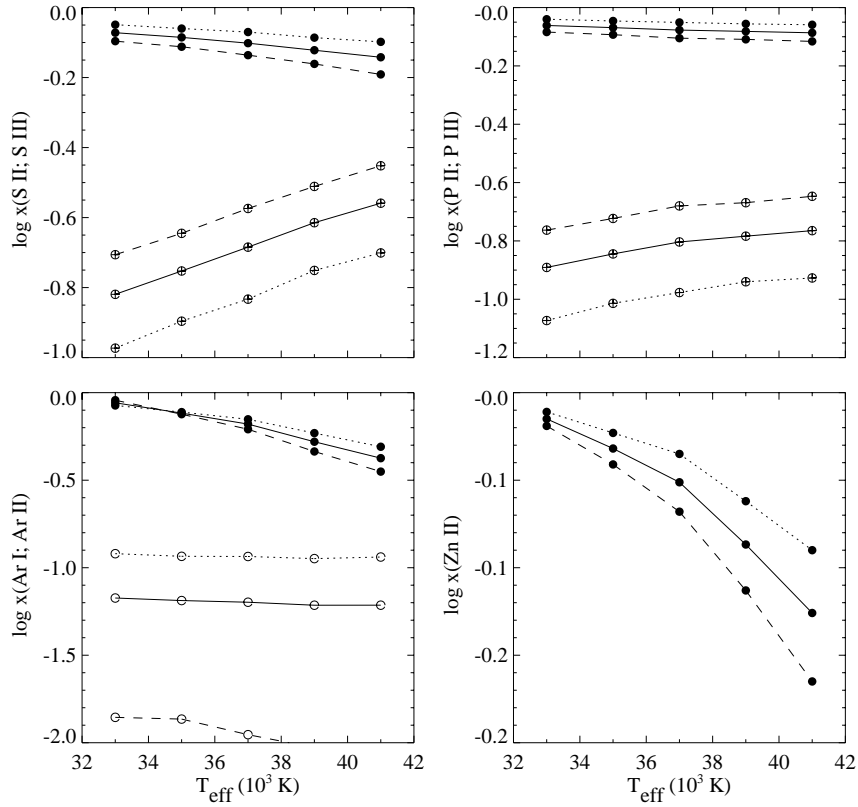


FIG. 2b

FIG. 2.—Volume-averaged ionization fractions, $\log x(X^i)$, vs. input stellar effective temperature of the ionizing central source in our nebular models with WNM abundance patterns. The curves shown are for the $x_{\text{edge}} = 0.10$ (dashed lines), $x_{\text{edge}} = 0.95$ (dotted lines), and composite (solid lines) cases. Ionization stages (I, open circles; II, filled circles; III, crossed circles) are shown for (a) He, C, N, and O, (b) S, P, Ar, and Zn, (c) Si, Mg, Mn, and Cr, and (d) Fe, Ti, Al, and Ni.

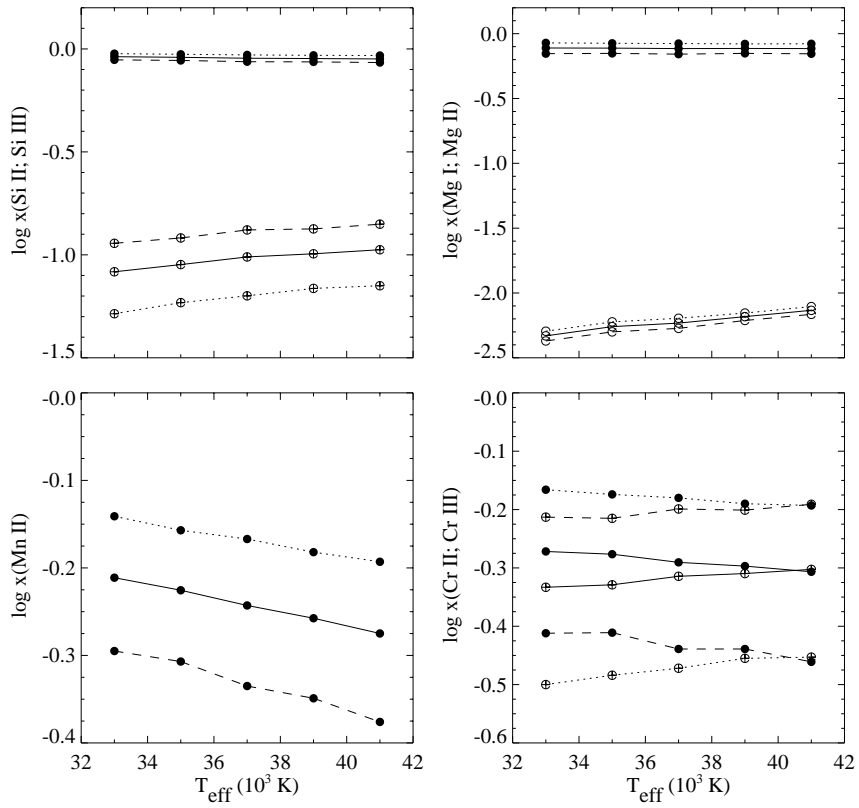


FIG. 2c

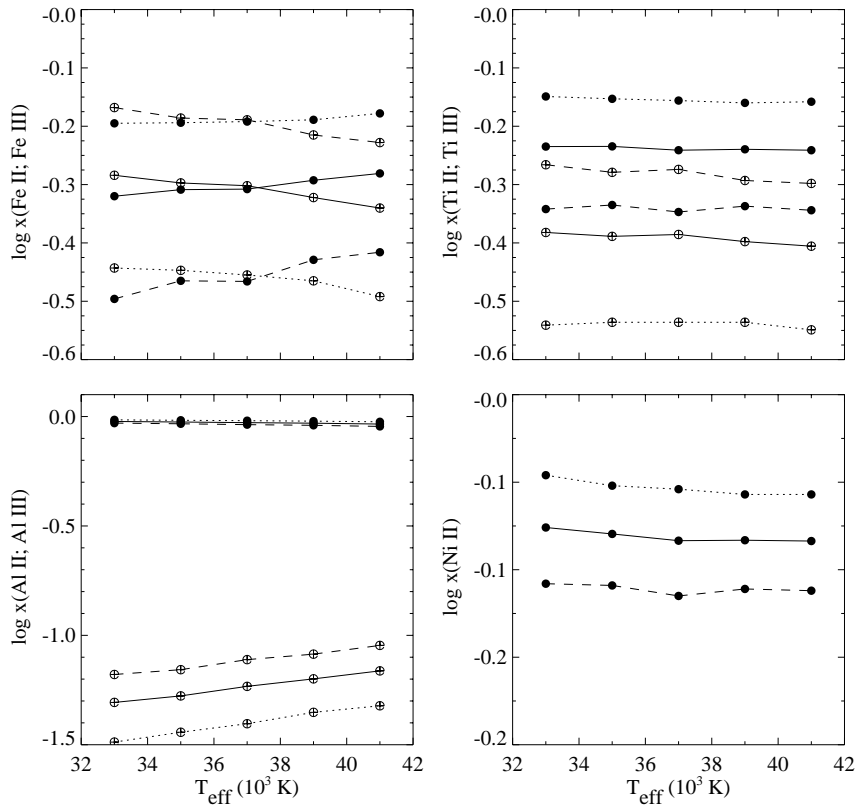


FIG. 2d

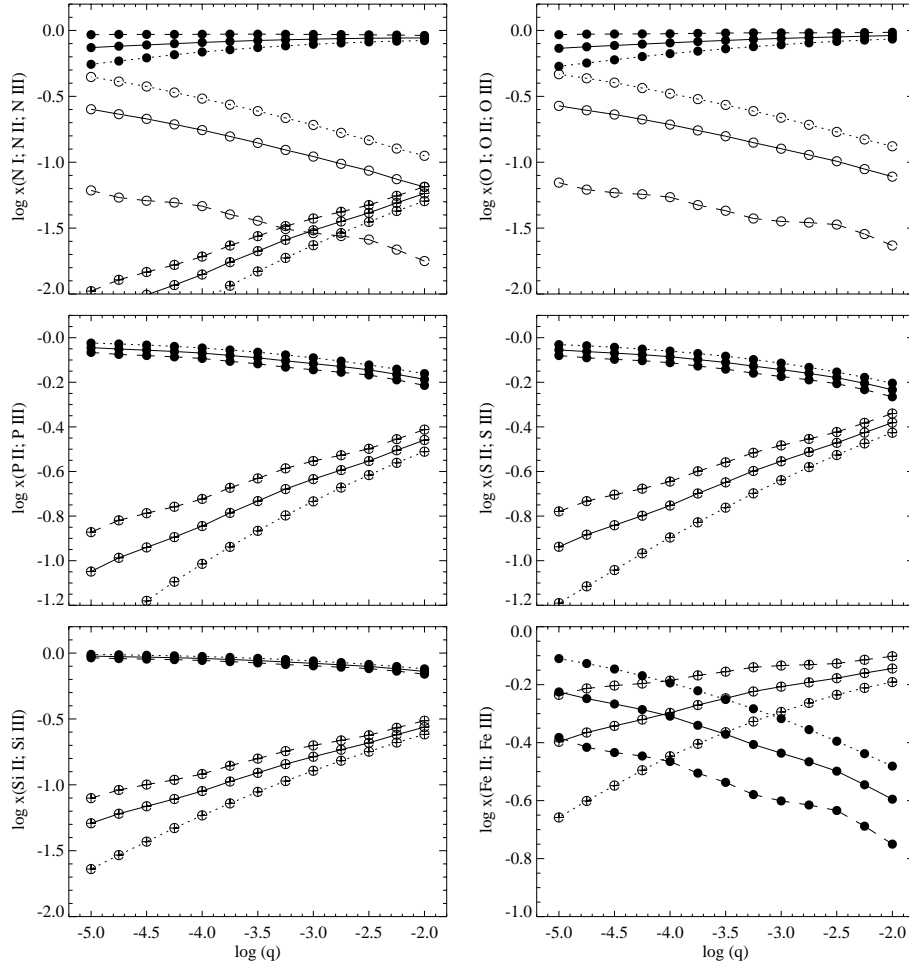


FIG. 3.—Volume-averaged ionization fractions, $\log x(X^i)$, vs. ionization parameter, $\log(q)$, for a model nebula with a WNM abundance pattern and an ionizing source characterized by $T_{\text{eff}} = 35,000$ K. The curves shown are for the $x_{\text{edgc}} = 0.10$ (dashed lines), $x_{\text{edgc}} = 0.95$ (dotted lines), and composite (solid lines) cases. Ionization stages I (open circles), II (filled circles), and III (crossed circles) are shown.

It is difficult to estimate $N(\text{H})_{\text{WIM}}$ directly since $N(\text{H}^+)$ is not directly observed, so a suitable proxy for $N(\text{H})_{\text{WIM}}$ may need to be found.

In the WNM, the column density of element X is equal to the observed value less the amount in the WIM, which is simply the sum of the individual contributions of X^i to $N(X)$ in the WNM:

$$N(X)_{\text{WNM}} = \sum_{i=0}^{j-1} \left[N(X^i) - \frac{x(X^i)}{x(X^j)} N(X^j) \right]. \quad (7)$$

In equation (7), the second term in parentheses accounts for the amount of X^i in the WIM. We use the following equations to estimate the amount of H I in the WIM (eq. [8]) and the WNM (eq. [9]):

$$F_H \approx 1 - \sum_{i=0}^{j-1} \left[\frac{N(X^i)_{\text{WNM}}}{N(X^i)} \right] \quad (8)$$

and

$$N(\text{H}^0)_{\text{WNM}} = N(\text{H}^0)[1 - x(\text{H}^0)F_H]. \quad (9)$$

In equations (8) and (9), F_H is the fraction of hydrogen along the sight line associated with the WIM. The ionization fraction of H I in the WIM, $x(\text{H}^0)$, in our models is $\sim 5\text{--}30\%$, so most of the H I is associated with the WNM.

Combining equations (6) and (8), we derive the logarithmic abundance of X relative to H in the WNM:

$$A(X)_{\text{WNM}} = \log \left| \frac{N(X)}{N(\text{H}^0)} \right|_{\text{WNM}} + 12.00. \quad (10)$$

4.2. An Example: The HD 93521 Sight Line

To demonstrate our approach we apply the method outlined in equations (3)–(10) to estimate the gas-phase abundance of S in the warm halo clouds toward HD 93521. Spitzer & Fitzpatrick (1993) have presented high-resolution observations of this sight line obtained with the Goddard High Resolution Spectrograph on board *HST*. The neutral and ionized species occur at very similar velocities along this sight line, so the contributions of ionized gas to the derived elemental abundances may be important. Spitzer & Fitzpatrick (1993) measured the column densities of S II, S III, and H I in the individual “warm fast” clouds along this sight line. In the first five columns of Table 7 we give their identifications, LSR velocities, and column densities of S II, S III, and H I for each of these clouds. These values are followed in column (6) by the column density of S II in the WIM calculated using equation (7) and the model predictions given in Table 5. The ratio of S II in the WNM to total

TABLE 7
STANDARD MODEL RESULTS FOR THE HD 93521 SIGHT LINE^a

Component (1)	$\langle V_{\text{LSR}} \rangle$ (km s ⁻¹) (2)	log $N(\text{S II})$ (3)	log $N(\text{S III})$ (4)	log $N(\text{H I})$ (5)	log $N(\text{S II})_{\text{WIM}}$ (6)	$\frac{N(\text{S II})_{\text{WNM}}}{N(\text{S II})}$ (7)	$\frac{N(\text{H I})_{\text{WNM}}}{N(\text{H I})}$ (8)	$A(\text{S})$ (9)	$A(\text{S}) - A_c(\text{S})$ (10)
Composite Model									
1	-66.3	14.09 ± 0.03	13.05 ± 0.21	18.85	13.71	0.58	0.92	7.04	-0.03
2	-57.8	14.50 ± 0.02	13.11 ± 0.22	19.26	13.77	0.81	0.97	7.17	+0.10
3	-51.2	14.53 ± 0.03	13.71 ± 0.07	19.29	14.37	0.31	0.87	6.79	-0.28
4	-38.8	14.02 ± 0.07	13.14 ± 0.31	18.78	13.80	0.40	0.89	6.89	-0.18
Sum	14.95 ± 0.02	13.95 ± 0.08	19.71	14.61	0.54	0.91	7.01	-0.06
$x_{\text{edge}} = 0.10$									
1	-66.3	14.09 ± 0.03	13.05 ± 0.21	18.85	13.59	0.68	0.94	7.08	+0.01
2	-57.8	14.50 ± 0.02	13.11 ± 0.22	19.26	13.65	0.86	0.97	7.18	+0.11
3	-51.2	14.53 ± 0.03	13.71 ± 0.07	19.29	14.25	0.48	0.90	6.93	-0.14
4	-38.8	14.02 ± 0.07	13.14 ± 0.31	18.78	13.68	0.54	0.91	6.98	-0.09
Sum	14.95 ± 0.02	13.95 ± 0.08	19.71	14.49	0.65	0.94	7.06	-0.01

^a Observed quantities [$\langle V_{\text{LSR}} \rangle$, $N(\text{S II})$, $N(\text{S III})$, $N(\text{H I})$] are measurements for the “warm, fast” halo clouds observed toward HD 93521 by Spitzer & Fitzpatrick 1993. The remaining derived quantities are defined in the text.

S II in each cloud is listed in column (7). Equations (8) and (9) were used to derive the ratio of H I in the WNM to the observed value. We list this ratio in column (8). Column (9) contains the derived abundance of S in the WNM found from equation (10), and column (10) contains $A(\text{S}) - A_c(\text{S})$, the logarithmic gas-phase abundance of sulfur relative to the WNM reference abundance given in Table 2.

Table 7 shows the results of these calculations using both the standard composite model and the $x_{\text{edge}} = 0.10$ model results for $x(X^i)$. The cloud-to-cloud scatter in the values of $A(\text{S}) - A_c(\text{S})$ is generally of the order of the measurement errors on $N(\text{S III})$. Values of $A(\text{S}) - A_c(\text{S})$ for components 1, 2, and 4 for the standard composite model are consistent with a negligible gas-phase depletion of S onto dust grains. The value for component 3 suggests either that there may be a small amount of S incorporated into dust or that the ionization properties or intrinsic abundances of cloud 3 vary enough to produce the observed deviation from the reference abundance. In the $x_{\text{edge}} = 0.10$ model, the -0.14 dex deviation from the reference value is a 2σ excursion. The cloud 3 value is 0.2 dex below the value of $A(\text{S})$ derived by Spitzer & Fitzpatrick (1993), who assumed that all of the S II in these clouds is associated with the H I (i.e., they did not apply any ionization corrections).

We find that a substantial ionization correction is necessary for S II to explain the amount of S III observed along the sight line. We find that roughly 50% of the S II is in the WNM, with the other 50% contained in the WIM (see Table 7). It is interesting that Spitzer & Fitzpatrick (1993) found an electron density for the HD 93521 clouds comparable to that of the WIM. The main difference in addressing ionization in these two studies is that they used the observed ratio $N(\text{S II})/N(\text{S III})$ and measured electron density to derive the photoionization rate for S II under conditions of photoionization equilibrium, whereas our results take into account the explicit ionizing spectrum required to match the WIM properties. We also predict varying ionization conditions between clouds, whereas they assumed constant properties. Spitzer & Fitzpatrick (1993) argued that the free electrons and neutral gas along the HD 93521 sight line are well mixed. Our calculation is consis-

tent with this result but does not require it. Additional observations of other ionized gas species in the HD 93521 clouds would help to characterize their ionization conditions and the impact of ionization on the derived elemental abundances.

Analyses such as these have also been used successfully to study the abundances in the WNM of the Galactic disk and halo and in intermediate-velocity clouds (e.g., Sembach 1995; Howk et al. 1999). Eventually, similar studies of the WIM abundances could be made (see Howk & Savage 1999). We note that especially good indicators of partially ionized gas are observable at the far-ultraviolet wavelengths to be observed by *FUSE*. Information about spectral lines that are useful probes of photoionized gas can be found in Sembach (1999) and Howk & Savage (1999); see Table 1 in both papers.

5. CONCLUDING REMARKS

The outlook for a better understanding of the abundances and physical properties of the WIM is bright. Advances in measuring the emission-line properties of the WIM will probably occur at optical and near-infrared wavelengths in the near future. Emission-line studies of the WIM at wavelengths $\lambda < 3000 \text{ \AA}$ will require sensitive detectors with large fields of view. The predicted intensities of the strongest emission lines at far-ultraviolet wavelengths ($\lambda < 1200 \text{ \AA}$) in our models are currently below the sensitivity of *FUSE*. In the standard composite model [C II] $\lambda 1020$, C III $\lambda 977$, N II $\lambda 1085$, and N III $\lambda 990$ all have intensities less than $10^{-2} I_{\text{H}\alpha}$. At these strengths, the far-ultraviolet WIM emission lines measured by *FUSE* in its $30'' \times 30''$ aperture should fall well below the expected background levels of $\sim 0.5 \text{ counts s}^{-1} \text{ cm}^{-2}$ and should pose no significant contamination problem for studies of hot gas emission (e.g., O VI) from the highly ionized ISM. Absorption-line studies of the WIM with *FUSE* should be feasible, with excellent diagnostics of photoionized gas ranging in ionization energies from 1 to 4 ryd (e.g., C II–III, N I–III, Ar I–II, Fe II–III, P II–IV, S III–IV).

The results of this work are applicable to warm ionized gas regions in other galaxies. A companion study of warm

ionized gas and its effects on elemental abundance determinations in damped Ly α absorbers can be found in Howk & Sembach (1999).

We thank Gary Ferland and his coworkers at the University of Kentucky for all of their work on the CLOUDY code. We also thank John Mathis for useful discussions

about modeling the WIM and Ron Reynolds for helpful suggestions for improving the manuscript. K. R. S. and J. C. H. acknowledge support from NASA Long Term Space Astrophysics grant NAG 5-3485 and grant GO-07270.01-96A from the Space Telescope Science Institute, which is operated by the Association of Universities for Research in Astronomy, Inc., under NASA contract NAS 5-26555.

APPENDIX

IONIZATION CORRECTIONS FOR LOW-DENSITY H II REGIONS

Although the main purpose of this work is to determine ionization fractions for the WIM of the Galaxy, our CLOUDY calculations also have applicability to studies of ionized gas in low-density H II regions. H II regions can be a significant source of singly ionized species, which are also the primary tracers of many elements in the neutral ISM. Howk et al. (1999) have discussed the effects of H II region gas on the study of the gas-phase abundances in the WNM along the μ Columbae sight line.

The data given in Table 5 describe the volume-averaged properties of our model nebulae. For a sight line through a diffuse H II region toward the central ionizing source, it may be more appropriate to use radially averaged ionization fractions (see Howk & Savage 1999). In Table 8 we list the radially averaged ionization fractions for all 20 elements considered in this study. We provide ionization fractions for diffuse H II regions characterized by $\log(q) = -3.0$ and -4.0 , with an ionizing spectrum from an ATLAS model atmosphere with $T_{\text{eff}} = 35,000$ K. We present model results for both $x_{\text{edge}} = 0.10$ and 0.95 . Figures 4a and 4b show the variations in these ionization fractions as a function of input stellar effective temperature for a select number of elements for the $\log(q) = -4.0$ models. For the elements Al, Si, Mg, Cr, and Mn, the variation in the ionization fractions of the singly and doubly ionized stages is less than 0.05 dex over the range $31,000 \text{ K} \leq T_{\text{eff}} \leq 41,000 \text{ K}$. Figure 5 shows the variation in ionization fraction with $\log(q)$, assuming an input spectrum with $T_{\text{eff}} = 35,000$ K.

Howk & Savage (1999) have tabulated radially average ionization fractions for a limited number of ions and discussed in detail how the ionization fractions vary with assumed model parameters. The results presented below are more thorough in the sense that more elements are covered, though over a smaller range of ionization parameter. These ionization fractions are appropriate for very low density H II regions. In particular, these results should be useful for studying contamination from H II

TABLE 8
IONIZATION FRACTIONS FOR LOW-DENSITY H II REGIONS^a

ELEMENT	$\log(q) = -3.0$						$\log(q) = -4.0$					
	$x_{\text{edge}} = 0.10$			$x_{\text{edge}} = 0.95$			$x_{\text{edge}} = 0.10$			$x_{\text{edge}} = 0.95$		
	I	II	III	I	II	III	I	II	III	I	II	III
H	-1.81	-0.01	...	-1.08	-0.04	...	-1.60	-0.01	...	-0.87	-0.06	...
He	-0.44	-0.20	-8.06	-0.34	-0.26	-8.13	-0.42	-0.21	-7.52	-0.28	-0.32	-7.63
C	-2.81	-0.17	-0.50	-2.71	-0.14	-0.57	-2.52	-0.12	-0.61	-2.37	-0.10	-0.72
N	-1.87	-0.14	-0.59	-1.13	-0.15	-0.66	-1.65	-0.10	-0.72	-0.90	-0.14	-0.83
O	-1.78	-0.05	-1.04	-1.07	-0.08	-1.11	-1.57	-0.04	-1.18	-0.85	-0.09	-1.30
Ne	-1.49	-0.02	-1.79	-1.11	-0.04	-1.86	-1.26	-0.03	-1.91	-0.86	-0.07	-2.02
Na	-2.28	-0.00	-3.02	-2.26	-0.00	-3.08	-2.14	-0.00	-2.88	-2.01	-0.01	-2.99
Mg	-2.71	-0.45	-0.19	-2.63	-0.36	-0.25	-2.52	-0.35	-0.26	-2.44	-0.25	-0.36
Al	-3.27	-0.18	-0.58	-3.29	-0.15	-0.65	-3.05	-0.13	-0.70	-3.03	-0.10	-0.80
Si	-4.05	-0.30	-0.32	-4.04	-0.24	-0.39	-3.88	-0.21	-0.42	-3.78	-0.16	-0.53
P	-3.02	-0.34	-0.29	-2.94	-0.28	-0.35	-2.67	-0.26	-0.37	-2.56	-0.19	-0.48
S	-3.48	-0.38	-0.24	-3.37	-0.31	-0.30	-3.13	-0.28	-0.33	-2.98	-0.21	-0.43
Ar	-2.42	-0.36	-0.26	-1.57	-0.30	-0.32	-2.21	-0.33	-0.28	-1.33	-0.26	-0.40
Ca	-3.08	-1.21	-0.03	-3.05	-1.14	-0.03	-2.64	-0.97	-0.05	-2.56	-0.85	-0.07
Ti	-3.74	-0.74	-0.20	-3.54	-0.55	-0.25	-3.51	-0.59	-0.22	-3.21	-0.39	-0.31
Cr	-4.04	-0.89	-0.12	-3.81	-0.63	-0.17	-3.76	-0.70	-0.14	-3.46	-0.44	-0.23
Mn	-2.32	-0.67	-0.15	-2.05	-0.51	-0.20	-2.00	-0.53	-0.19	-1.69	-0.37	-0.28
Fe	-4.03	-0.90	-0.16	-3.77	-0.64	-0.21	-3.75	-0.73	-0.17	-3.38	-0.47	-0.26
Ni	-2.56	-0.47	-0.21	-2.51	-0.37	-0.27	-2.28	-0.34	-0.30	-2.17	-0.24	-0.41
Zn	-2.57	-0.22	-0.41	-2.54	-0.18	-0.48	-2.41	-0.17	-0.50	-2.26	-0.13	-0.61

^a The ionization fraction of an ion X^i is given by $x(X^i) = N(X^i)/N(X_{\text{total}})$. We present radially averaged values of $\log x(X^i)$ for the first three ionization states of each element. Each model assumes WNM abundances (see Table 2) and a stellar input spectrum characterized by $T_{\text{eff}} = 35,000$ K and $\log(q) = 4.0$. Results are listed for ionization parameters of $\log(q) = -3.0$ and -4.0 .

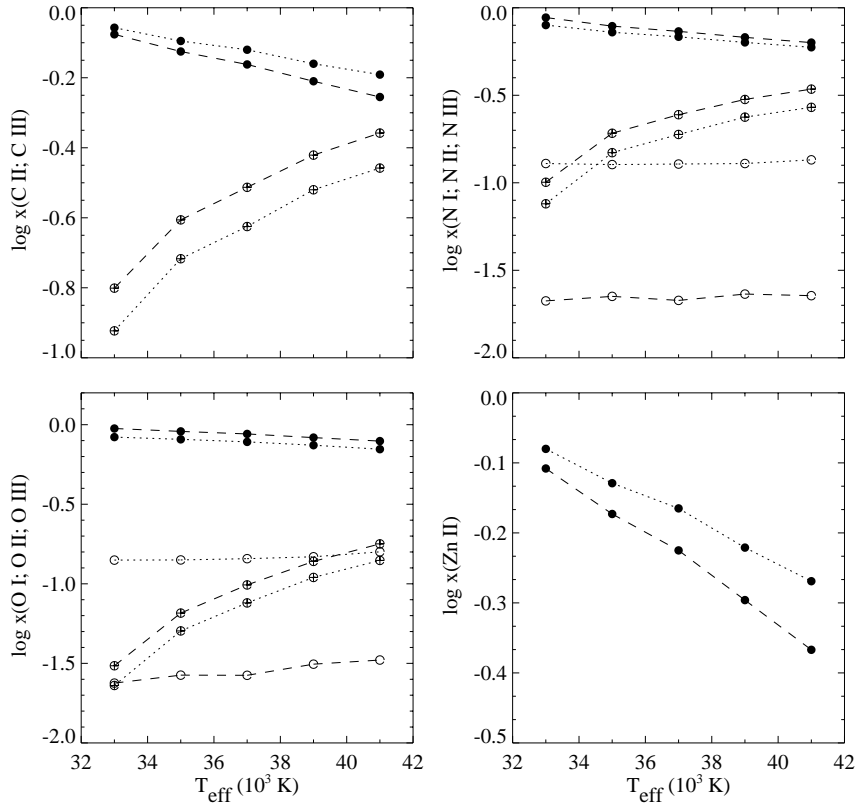


FIG. 4a

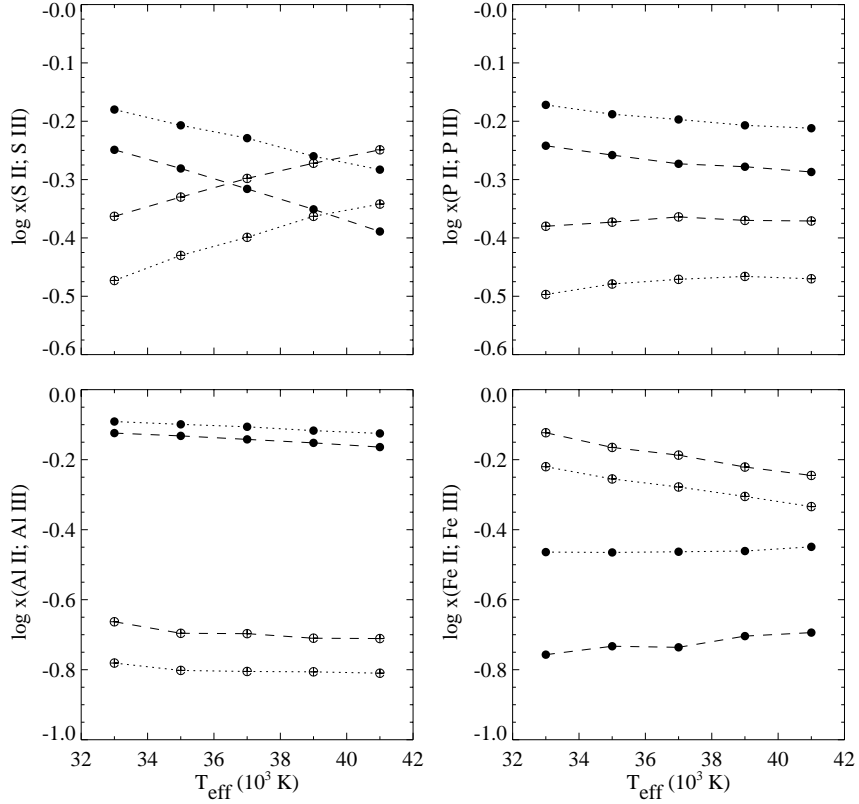


FIG. 4b

FIG. 4.—Radially averaged ionization fractions, $\log x(X^i)$, vs. effective temperature assumed for the ionizing central star. The curves shown are for the $x_{\text{edge}} = 0.10$ (dashed lines) and $x_{\text{edge}} = 0.95$ (dotted lines) models. All models assume WNM abundance patterns but the ionization fractions are relatively insensitive to the adopted abundances. Ionization stages (I, open circles; II, filled circles; III, crossed circles) are shown for (a) C, N, O, and Zn and (b) S, P, Fe, and Al.

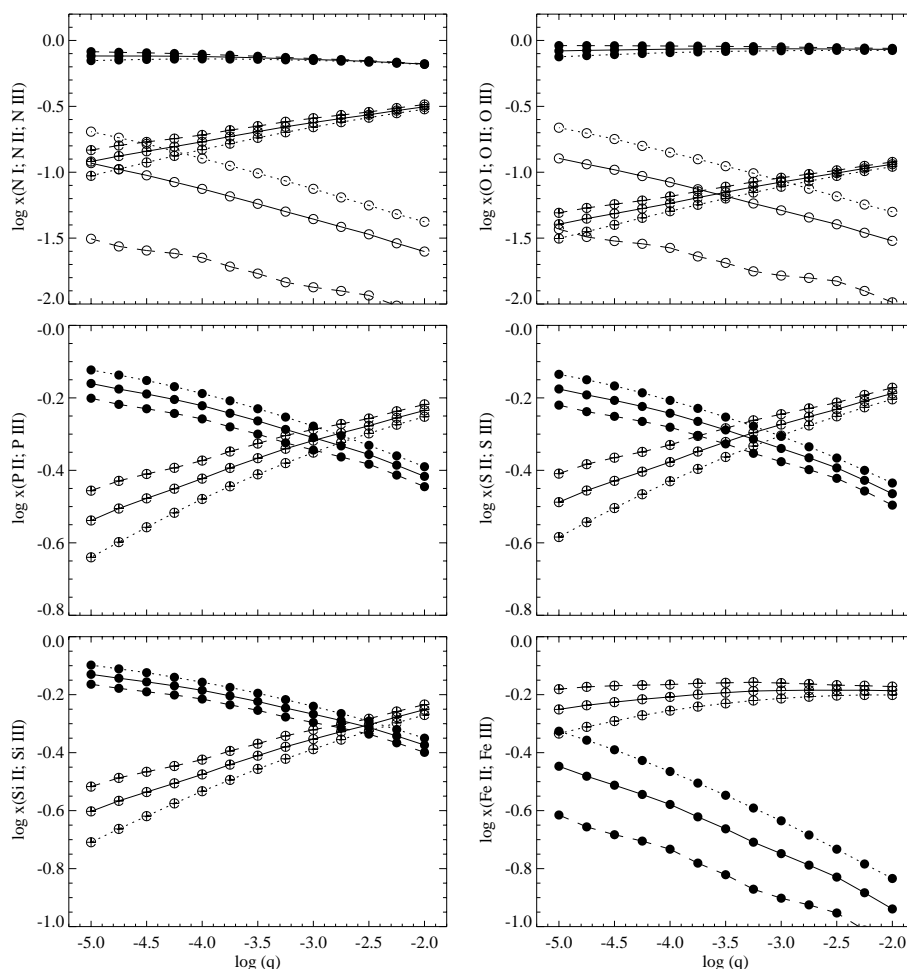


FIG. 5.—Radially averaged ionization fractions, $\log x(X^I)$, vs. ionization parameter, $\log(q)$. The curves shown are for the $x_{\text{edge}} = 0.10$ (dashed lines) and $x_{\text{edge}} = 0.95$ (dotted lines) models. These models assume an ionizing central star with $T_{\text{eff}} = 35,000$ K. All models assume WNM abundance patterns, but the ionization fractions are relatively insensitive to the adopted abundances. Ionization stages I (open circles), II (filled circles), and III (crossed circles) are shown.

regions surrounding early-type stars at large distances from the Galactic plane or along short, low-density sight lines where an appreciable number of additional H II regions have not been intercepted.

The application of the ionization fractions given in Table 8 should be approached in a method similar to that described in § 4. When possible, multiple observations of adjacent ions should be used to constrain the most appropriate model parameters. The radially averaged values tend to favor higher ionization gas than the volume-averaged results since the partially ionized outer regions of the nebula are given less weight in the averaging process.

REFERENCES

- Anders, E., & Grevesse, N. 1989, *Geochim. Cosmochim. Acta*, 53, 197
 Baldwin, J., Ferland, G. J., Martin, P. G., Corbin, M., Cota, S., Peterson, B. M., & Slettebak, A. 1991, *ApJ*, 374, 580
 Bland-Hawthorn, J., & Maloney, P. R. 1999, *ApJ*, 510, L33
 Cox, D. P., & Reynolds, R. J. 1992, *ApJ*, 400, L33
 Dettmar, R. J. 1990, *A&A*, 232, L15
 Dickey, J. M., & Lockman, F. J. 1990, *ARA&A*, 28, 215
 Domgörgen, H., & Mathis, J. S. 1994, *ApJ*, 428, 647
 Dove, J. B., & Shull, J. M. 1994, *ApJ*, 430, 222
 Ferland, G. J. 1996, *HAZY*, a Brief Introduction to CLOUDY 90, Internal Report (Univ. Kentucky Dept. Phys. Astron.)
 Ferland, G., et al. 1994, in *The Analysis of Emission Lines: A Meeting in Honor of the 70th Birthdays of D. E. Osterbrock and M. J. Seaton*, ed. R. Williams & M. Livio (Cambridge: Cambridge Univ. Press), 83
 Ferland, G. J., Korista, K. T., Verner, D. A., Ferguson, J. W., Kingdon, J. B., & Verner, E. M. 1998, *PASP*, 110, 761
 Grevesse, N., & Noels, A. 1993, in *Origin and Evolution of the Elements*, ed. N. Prantzos, E. Vangioni-Flam, & M. Cassé (Cambridge: Cambridge Univ. Press), 15
 Haffner, L. M., Reynolds, R. J., & Tufté, S. L. 1999, *ApJ*, 523, 223
 Hoopes, C. G., Walterbos, R. A. M., & Rand, R. J. 1999, *ApJ*, 522, 669
 Howk, J. C., & Savage, B. D. 1999, *ApJ*, 517, 746
 Howk, J. C., Savage, B. D., & Fabian, D. 1999, *ApJ*, 525, 253
 Howk, J. C., & Sembach, K. R. 1999, *ApJ*, 523, L141
 Kilian-Montenbruck, J., Gehren, T., & Nissen, P. E. 1994, *A&A*, 291, 757
 Kurucz, R. L. 1991, in *Proc. Workshop on Precision Photometry: Astrophysics of the Galaxy*, ed. A. C. Davis Philip, A. R. Upgren, & K. A. James (Schenectady: Davis), 27
 Lagache, G., Abergel, A., Boulanger, F., Désert, F. X., & Puget, J.-L. 1999, *A&A*, 344, 322
 Maloney, P. R., & Bland-Hawthorn, J. 1999, in *ASP Conf. Ser. 166, Proc. Stromlo Workshop on High-Velocity Clouds*, ed. B. K. Gibson & M. E. Putnam (San Francisco: ASP), 199
 Mathis, J. S. 1996, *ApJ*, 472, 643
 Meyer, D. M., Cardelli, J. A., & Sofia, U. J. 1997, *ApJ*, 490, L103
 Meyer, D. M., Jura, M., & Cardelli, J. A. 1998, *ApJ*, 493, 222
 Miller, W. W., & Cox, D. P. 1993, *ApJ*, 417, 579
 Minter, A. H., & Balser, D. S. 1997, *ApJ*, 484, L133
 Moore, C. E. 1970, *Ionization Potentials and Ionization Limits Derived from the Analysis of Optical Spectra* (NSRDS-NBS Rep. 34; Washington, DC: NBS)
 Ogdén, P. M., & Reynolds, R. J. 1985, *ApJ*, 290, 238
 Osterbrock, D. E. 1989, *Astrophysics of Gaseous Nebulae and Active Galactic Nuclei* (Mill Valley: University Science)

- Peimbert, M., Torres-Peimbert, S., & Ruiz, M. T. 1992, *Rev. Mexicana Astron. Astrofis.*, 24, 155
- Rand, R. J. 1996, *ApJ*, 462, 712
- Rand, R. J., Kulkarni, S. R., & Hester, J. J. 1990, *ApJ*, 352, L1
- . 1992, *ApJ*, 396, 97
- Raymond, J. C. 1992, *ApJ*, 384, 502
- Reynolds, R. J. 1985a, *ApJ*, 294, 256
- . 1985b, *ApJ*, 298, L27
- . 1993, in *Back to the Galaxy*, ed. S. Holt & F. Verter (New York: AIP), 156
- Reynolds, R. J., Hausen, N. R., Tufte, S. L., & Haffner, L. M. 1998a, *ApJ*, 494, L99
- Reynolds, R. J., Roessler, F. L., & Scherb, F. 1977, *ApJ*, 211, 115
- Reynolds, R. J., & Tufte, S. L. 1995, *ApJ*, 439, L17
- Reynolds, R. J., Tufte, S. L., Haffner, L. M., Jaehnig, K., & Percival, J. W. 1998b, *Publ. Astron. Soc. Australia*, 15, 14
- Savage, B. D., & Sembach, K. R. 1996, *ARA&A*, 34, 279
- Sembach, K. R. 1995, *ApJ*, 445, 314
- . 1999, in *ASP Conf. Ser. 163, Proc. Stromlo Workshop on High Velocity Clouds*, ed. B. K. Gibson & M. E. Putnam (San Francisco: ASP), 243
- Slavin, J. D., Shull, J. M., & Begelman, M. C. 1993, *ApJ*, 407, 83
- Snow, T. P., & Witt, A. N. 1996, *ApJ*, 468, L65
- Sofia, U. J., Cardelli, J. A., Guerin, K. P., & Meyer, D. M. 1997, *ApJ*, 482, L105
- Spitzer, L., & Fitzpatrick, E. L. 1993, *ApJ*, 409, 299
- Vacca, W. D., Garmany, C. D., & Shull, J. M. 1996, *ApJ*, 460, 914